

Brain Gliomas: Multicenter Standardized Assessment of Dynamic Contrast-enhanced and Dynamic Susceptibility Contrast MR Images¹

Nicoletta Anzalone, MD
 Antonella Castellano, MD, PhD
 Marcello Cadioli, MSc
 Gian Marco Conte, MD
 Valeria Cuccharini, MD
 Alberto Bizzi, MD
 Marco Grimaldi, MD
 Antonella Costa, MD
 Giovanni Grillea, MD
 Paolo Vitali, MD, PhD
 Domenico Aquino, MSc
 Maria Rosa Terreni, MD
 Valter Torri, MD
 Bradley J. Erickson, MD, PhD
 Massimo Caulo, MD, PhD

¹ From the Neuroradiology Unit and CERMAC, Vita-Salute San Raffaele University and IRCCS San Raffaele Scientific Institute, Via Olgettina 60, 20132, Milan, Italy (N.A., A. Castellano, M. Cadioli, G.M.C.); Neuroradiology Unit, Fondazione IRCCS Istituto Neurologico Carlo Besta, Milan, Italy (V.C., A.B., D.A.); Department of Radiology, Humanitas Clinical and Research Hospital, Rozzano, Milan, Italy (M.G.); Department of Neuroradiology, Fondazione IRCCS Cà Granda-Ospedale Maggiore Policlinico, Milan, Italy (A. Costa); IRCCS Neuromed, Pozzilli (Isernia), Italy (G.G.); Neuroradiology Unit, C. Mondino National Neurologic Institute, Pavia, Italy (P.V.); Pathology Unit, IRCCS San Raffaele Scientific Institute, Milan, Italy (M.R.T.); Methodology for Clinical Research Laboratory, Department of Oncology, IRCCS Mario Negri, Milan, Italy (V.T.); Department of Radiology, Mayo Clinic, Rochester, Minn (B.J.E.); and Department of Neuroscience and Imaging and ITAB-Institute of Advanced Biomedical Technologies, University G. d'Annunzio, Chieti, Italy (M. Caulo). Received February 15, 2017; revision requested May 22; revision received September 13; accepted October 2; final version accepted October 27. **Address correspondence to** N.A. (e-mail: anzalone.nicoletta@hsr.it).

Supported by Bayer Healthcare.

© RSNA, 2018

Purpose:

To evaluate the feasibility of a standardized protocol for acquisition and analysis of dynamic contrast material-enhanced (DCE) and dynamic susceptibility contrast (DSC) magnetic resonance (MR) imaging in a multicenter clinical setting and to verify its accuracy in predicting glioma grade according to the new World Health Organization 2016 classification.

Materials and Methods:

The local research ethics committees of all centers approved the study, and informed consent was obtained from patients. One hundred patients with glioma were prospectively examined at 3.0 T in seven centers that performed the same preoperative MR imaging protocol, including DCE and DSC sequences. Two independent readers identified the perfusion hotspots on maps of volume transfer constant (K^{trans}), plasma (v_p) and extravascular-extracellular space (v_e) volumes, initial area under the concentration curve, and relative cerebral blood volume (rCBV). Differences in parameters between grades and molecular subtypes were assessed by using Kruskal-Wallis and Mann-Whitney U tests. Diagnostic accuracy was evaluated by using receiver operating characteristic curve analysis.

Results:

The whole protocol was tolerated in all patients. Perfusion maps were successfully obtained in 94 patients. An excellent interreader reproducibility of DSC- and DCE-derived measures was found. Among DCE-derived parameters, v_p and v_e had the highest accuracy (are under the receiver operating characteristic curve [A_z] = 0.847 and 0.853) for glioma grading. DSC-derived rCBV had the highest accuracy (A_z = 0.894), but the difference was not statistically significant ($P > .05$). Among lower-grade gliomas, a moderate increase in both v_p and rCBV was evident in isocitrate dehydrogenase wild-type tumors, although this was not significant ($P > .05$).

Conclusion:

A standardized multicenter acquisition and analysis protocol of DCE and DSC MR imaging is feasible and highly reproducible. Both techniques showed a comparable, high diagnostic accuracy for grading gliomas.

©RSNA, 2018

Online supplemental material is available for this article.

Perfusion magnetic resonance (MR) imaging techniques are widely used in the clinical work-up of brain tumors because of their ability to help quantify tumor microvessel proliferation and permeability and thus to measure changes associated with neoangiogenesis, which correlate with tumor malignancy. In particular, dynamic susceptibility contrast (DSC) MR imaging (1) has been extensively explored for glioma grading (2), for prognostic assessment (3), and for differentiating between recurrent tumor and post-treatment changes (4). However, the lack of acquisition and analysis standardization of DSC has partly limited its inclusion in protocol guidelines for brain tumor diagnosis (5). Recently, a white paper on consensus recommendations for clinical performance of DSC

MR imaging has been published (6). Nonetheless, the low reproducibility among different softwares still remains an open issue (7–9).

Dynamic contrast material-enhanced (DCE) MR imaging has been recently introduced in the preoperative assessment and follow-up of brain tumors. The DCE signal intensity–time curve reflects a combination of tissue perfusion, microvessel permeability, and extravascular-extracellular space (5,10), thus allowing for a multi-parametric characterization of tumor microvasculature. The advantages of DCE over DSC are fewer susceptibility artifacts and the quantification of blood-brain barrier (BBB) integrity; indeed, the main interest for DCE-derived metrics was initially focused on the volume transfer constant (K^{trans}), a permeability marker correlating with BBB disruption (10) and malignancy (11,12). By introducing two-compartment pharmacokinetic models to fit DCE data, the plasma volume or fractional volume of the intravascular compartment (v_p) was also evaluated for glioma grading as a marker for tumor neoangiogenesis (13,14), and the fractional volume of the extravascular-extracellular space (v_e) was evaluated as a potential correlate of mitotic activity (15). The advantage of DSC over DCE is better temporal resolution, allowing better estimation of blood volume. Thus, each technique has strengths that may be valuable in glioma grading.

To date, a number of single-center studies reported a similar accuracy of DSC and DCE in glioma grading (16–19), mostly focused on DCE-derived K^{trans} . Nonetheless, a comprehensive evaluation of the accuracy of all DCE-derived metrics is still not available in the literature, and, consequently, the value of using either marker or the combination is not clear. Moreover, standardization of DCE acquisition and postprocessing protocols in a multicenter setting is still lacking.

This study aimed to evaluate a standardized protocol for acquisition and analysis of DSC and DCE data in a multicenter clinical setting and

to assess the accuracy of quantitative metrics derived from these techniques in predicting glioma grade, alone or in combination. A secondary aim was to explore the correlation of these metrics with common molecular alterations identified in the new 2016 World Health Organization (WHO) classification of gliomas (20).

Materials and Methods

Patients

The local research ethics committees of all centers approved the study, and all patients provided signed informed consent prior to MR imaging.

From June 2012 to June 2015, 100 consecutive adult patients (mean age,

Implications for Patient Care

- Although the use of dynamic susceptibility contrast (DSC) and dynamic contrast material-enhanced (DCE) perfusion MR imaging techniques to characterize gliomas is not new, the application to the new World Health Organization 2016 classification and correlation with molecular markers, with standardization and validation in a large multicenter cohort, has important future potential for clinical impact by stratifying patients with brain tumors into prognostic and/or treatment-response groups, especially for multicenter trials.
- A standardized protocol for acquisition and analysis of DSC and DCE perfusion MR imaging data is feasible in a multicenter clinical setting, showing a high reproducibility across different MR equipment and excellent inter-reader reproducibility of DSC- and DCE-derived measures.
- DCE and DSC techniques perform similarly in the preoperative grading of gliomas, thus supporting a more widespread inclusion of DCE in the clinic.

<https://doi.org/10.1148/radiol.2017170362>

Content codes: **MR** **NR**

Radiology 2018; 000:1–11

Abbreviations:

A_z = area under the ROC curve
 BBB = blood-brain barrier
 CBV = cerebral blood volume
 DCE = dynamic contrast enhanced
 DSC = dynamic susceptibility contrast
 iAUC = initial area under the concentration curve
 IDH = isocitrate dehydrogenase
 K^{trans} = volume transfer constant
 rCBV = relative CBV
 ROC = receiver operating characteristic
 ROI = region of interest
 v_e = fractional volume of the extravascular-extracellular space
 v_p = fractional volume of the intravascular compartment
 WHO = World Health Organization

Author contributions:

Guarantors of integrity of entire study, N.A., M.G., A. Costa, M.R.T., M.C.; study concepts/study design or data acquisition or data analysis/interpretation, all authors; manuscript drafting or manuscript revision for important intellectual content, all authors; manuscript final version approval, all authors; agrees to ensure any questions related to the work are appropriately resolved, all authors; literature research, N.A., A. Castellano, G.M.C., A.B., M.G., A. Costa, M.R.T.; clinical studies, N.A., A. Castellano, M. Cadioli, V.C., A.B., M.G., A. Costa, G.G., P.V., M.R.T., M.C.; experimental studies, N.A., A. Castellano, G.M.C., V.C., M.G., A. Costa, P.V., D.A., M.C.; statistical analysis, N.A., A. Castellano, G.M.C., M.G., A. Costa, V.T.; and manuscript editing, N.A., A. Castellano, M. Cadioli, G.M.C., V.C., A.B., M.G., A. Costa, P.V., V.T., B.J.E., M.C.

Conflicts of interest are listed at the end of this article.

52 years; range, 20–80 years; 62 men, 38 women) with a newly detected brain lesion suggestive of glioma at a previous computed tomographic (CT) or MR imaging examination were prospectively recruited in seven Italian centers (Ospedale San Raffaele, Milan; Ospedale Maggiore Policlinico, Milan; Istituto Neurologico Carlo Besta, Milan; Istituto Neurologico Mondino, Pavia; Humanitas Clinical and Research Hospital, Milan; Neuromed, Pozzilli; and ITAB, Chieti). All centers had a 3.0-T MR system and an 8- or 32-channel head coil: four Achieva imagers (Philips Healthcare, Best, the Netherlands), two Magnetom (Verio and Skyra) imagers (Siemens Healthcare, Erlangen, Germany), and one Signa HDxt system (GE Healthcare, Milwaukee, Wis). Bayer Healthcare (Berlin, Germany) gave financial support for running the study; the authors had complete control and property of the study data and of all the information submitted for publication.

Results in 20 of the 100 patients have been previously reported in a prior single-center study (16). However, the results did not influence this study, as here we report on the application of the standardized DSC and DCE protocol in a multicenter clinical setting.

Exclusion criteria were the presence of severe renal failure, a known allergy to gadolinium-based contrast agents, and corticosteroid administration in the week before the MR imaging study.

All patients underwent preoperative MR imaging that included conventional sequences and DSC and DCE imaging within 2 weeks before surgical resection or biopsy at the neurosurgical department of each participating center, where experienced neuropathologists provided the histopathologic diagnosis according to the WHO 2016 classification (20).

In 67 of the total cohort of patients, an integrated molecular analysis was provided, including immunohistochemistry and DNA sequencing to detect isocitrate dehydrogenase (IDH) mutations and fluorescence in situ hybridization to detect 1p/19q codeletion.

MR Imaging Protocol

A standardized MR imaging protocol including DSC and DCE acquisitions was implemented across the seven centers by using a previously described study design (16,17) and adapting the parameters to the different MR equipment (Table 1).

A fixed dose of 10 mL of gadobutrol (Gadovist, 1 mmol/mL; Bayer Healthcare, Berlin, Germany) was administered, divided into two equal parts of 5 mL. The first bolus was injected 50 seconds after the start of DCE acquisition, at a rate of 2 mL/sec. The second bolus was injected 16 seconds after the start of DSC acquisition, at a rate of 5 mL/sec. Each bolus was followed by a 20-mL saline flush. Thus, the first bolus during DCE presaturated the tissue to reduce the T1 contamination for the following DSC MR imaging study.

MR Imaging Data Analysis

All MR imaging studies were centralized after anonymization and processed by using the nordicICE software package (NordicNeuroLab, Bergen, Norway). Two board-certified neuroradiologists (N.A. and A. Castellano, with 20 and 10 years of experience, respectively), both blinded to histopathologic findings, independently evaluated all MR imaging studies and performed DSC and DCE analysis.

For DCE, patient-specific baseline T1 maps were derived from variable flip angle sequences (three flip angles: 5°, 10°, and 15°) by using the “T1 relaxation analysis” module of nordicICE. Deconvolution with a vascular input function (VIF) was performed by positioning a region of interest (ROI) for VIF selection in the superior sagittal sinus at the level of the lateral ventricles. The maps of v_p , K^{trans} , v_e , and initial area under the concentration curve (iAUC) were calculated by using the two-compartment extended Tofts model (10,21).

For DSC, cerebral blood volume (CBV) maps were calculated by using an established tracer kinetic model applied to the first-pass data, as implemented

in nordicICE. A semiautomatic arterial vascular input function was obtained in the middle cerebral arteries. Contrast agent leakage correction for the CBV was performed by using the first bolus injection and linear fitting to estimate the T1 contamination by contrast material extravasation (22). DCE- and DSC-derived parametric maps were coregistered to the anatomic data sets by using a rigid transformation.

The two independent readers drew four ROIs of 25–30 mm² on the DSC and DCE postprocessed images based on visual inspection, taking care to avoid normal vessels. Of the four ROIs, the ROI with the highest mean value was then used as the ROI for that image (hotspot). The highest CBV was divided by the CBV in a reference ROI in the contralateral normal-appearing white matter of the centrum semiovale to compute relative CBV (rCBV).

Statistical Analysis

Statistical analysis was performed by using Graph Pad Prism 6 (Graph Pad, San Diego, Calif), SPSS 20.0 for MacOSX (SPSS, IBM, Chicago, Ill) and MedCalc software, version 16.4.2 (MedCalc, Ostend, Belgium). $P < .05$ was considered to indicate a statistically significant difference. Interreader reproducibility of the DCE- and DSC-derived measures was assessed by using intraclass correlation coefficients. A required sample size of 92 was calculated on the basis of the probability of erroneously concluding accuracy of more than 74% at 10% (one-sided $\alpha = .096$) and the probability of correctly concluding this proportion was 80% or more at 90% ($\beta = 0.091$). Assuming a 10% dropout rate, we attempted to enroll approximately 100 patients.

Because of the nonnormal distribution of the variables, nonparametric statistics were used. The Kruskal-Wallis and Dunn multiple pairwise comparison tests were used to assess group differences in perfusion parameters between the three WHO grades (II, III, and IV). The Mann-Whitney U test was used to assess group differences in perfusion parameters between lower-grade gliomas and glioblastomas (II or III vs IV) and among lower-grade

Table 1

Parameters of MR Imaging Acquisition Protocol with Different MR Equipment

MR Imaging Unit, Acquisition Order, and Sequence

MR Imaging Unit, Acquisition Order, and Sequence	TR (msec)	TE (msec)	TI (msec)	Flip Angle (degrees)	No. of Dynamics	Acquisition Matrix	Thickness (mm)	Acquisition Time
Philips Achieva 3.0 T								
1. Axial T2-weighted TSE	3000	80	...	90	...	400 × 512	5	1 min 54 sec
2. Axial 3D FLAIR TSE	10000	110	2750	90	...	224 × 256	2.5	8 min 20 sec
3. Axial 3D spoiled gradient echo T1 weighted	7.2	3.5	...	8	...	256 × 256	2.5	1 min 22 sec
4. Axial spoiled gradient echo VFA	3.9	1.9	...	5, 10, 15	...	96 × 112	2.5	2 min 3 sec
5. Axial DCE 3D spoiled gradient echo T1 weighted	3.9	1.8	...	15	70	96 × 84	2.5	6 min 10 sec
6. Axial DSC FFE-EPI T2* weighted	1500	40	...	75	80	96 × 77	5	2 min 4 sec
7. Postcontrast axial 3D spoiled gradient echo T1 weighted	7.2	3.5	...	8	...	256 × 256	2.5	1 min 22 sec
Siemens Magnetom Verio and Skyra 3.0 T								
1. Axial T2-weighted TSE	5000	79	...	90	...	383 × 448	5	1 min 50 sec
2. Axial 3D FLAIR TSE	5500	502	1800	90	...	256 × 256	1	7 min 42 sec
3. Axial 3D spoiled gradient echo T1 weighted	1800	2.7	...	9	...	256 × 256	2.5	5 min 47 sec
4. Axial spoiled gradient echo VFA	3.9	1.9	...	5, 10, 15	...	96 × 112	2.5	2 min 3 sec
5. Axial DCE 3D spoiled gradient echo T1 weighted	3.9	1.8	...	15	70	96 × 86	5	6 min
6. Axial DSC FFE EPI T2* weighted	1500	31	...	75	80	96 × 91	5	2 min 8 sec
7. Postcontrast axial 3D spoiled gradient echo T1 weighted	1800	2.7	...	9	...	256 × 256	2.5	5 min 47 sec
GE Signa HDxt 3.0 T								
1. Axial T2-weighted TSE	3000	104	...	90	...	216 × 488	5	1 min 36 sec
2. Axial 3D FLAIR TSE	10000	151	2250	90	...	224 × 320	5	4 min
3. Axial 3D spoiled gradient echo T1 weighted	10.2	4.6	...	8	...	256 × 256	2.5	1 min 2 sec
4. Axial spoiled gradient echo VFA	3.9	1.9	...	5, 10, 15	...	96 × 112	2.5	1 min
5. Axial DCE 3D spoiled gradient echo T1 weighted	6.9	2.1	...	15	70	96 × 84	5	6 min 27 sec
6. Axial DSC FFE EPI T2* weighted	1500	40	...	75	80	92 × 108	5	2 min
7. Postcontrast axial 3D spoiled gradient echo T1 weighted	10.2	4.6	...	8	...	256 × 256	2.5	1 min 2 sec

Note.—DCE = dynamic contrast enhanced, DSC = dynamic susceptibility contrast, EPI = echo-planar imaging, FFE = fast field echo, FLAIR = fluid-attenuated inversion recovery, 3D = three-dimensional, TE = echo time, TI = inversion time, TR = repetition time, TSE = turbo spin-echo, VFA = variable flip angle.

gliomas according to IDH mutational status and 1p19q codeletion. The Benjamini-Hochberg method was used to adjust *P* values to account for multiple testing. The Spearman rank correlation coefficient (ρ) was used to assess the relationships between hotspot parameters and WHO grade.

Receiver operating characteristic (ROC) analysis was used to evaluate the diagnostic accuracy of each parameter by comparing the areas under the ROC curves (A_z values) in discriminating WHO IV glioblastoma from WHO

II or III lower-grade gliomas, according to the WHO 2016 classification scheme, as well as in discriminating WHO III or IV from WHO II gliomas, according to the previous WHO grading system. Cutoff values were selected for each parameter corresponding to a minimum sensitivity of 85% and a likelihood ratio higher than 3. Logistic regression analysis and ROC curves were calculated by combining DCE- and DSC-derived parameters to determine their added value for predicting glioma grade. The diagnostic accuracy of the

same parameters for distinguishing WHO II from III and WHO III from IV was also evaluated. Differences in perfusion parameters according to MR imaging vendor were assessed by using the Mann-Whitney U test.

Results

A total of 100 patients met the outlined inclusion and exclusion criteria and were recruited to this study. After the processing of DSC- and DCE-derived perfusion maps, six patients were excluded from

Figure 1

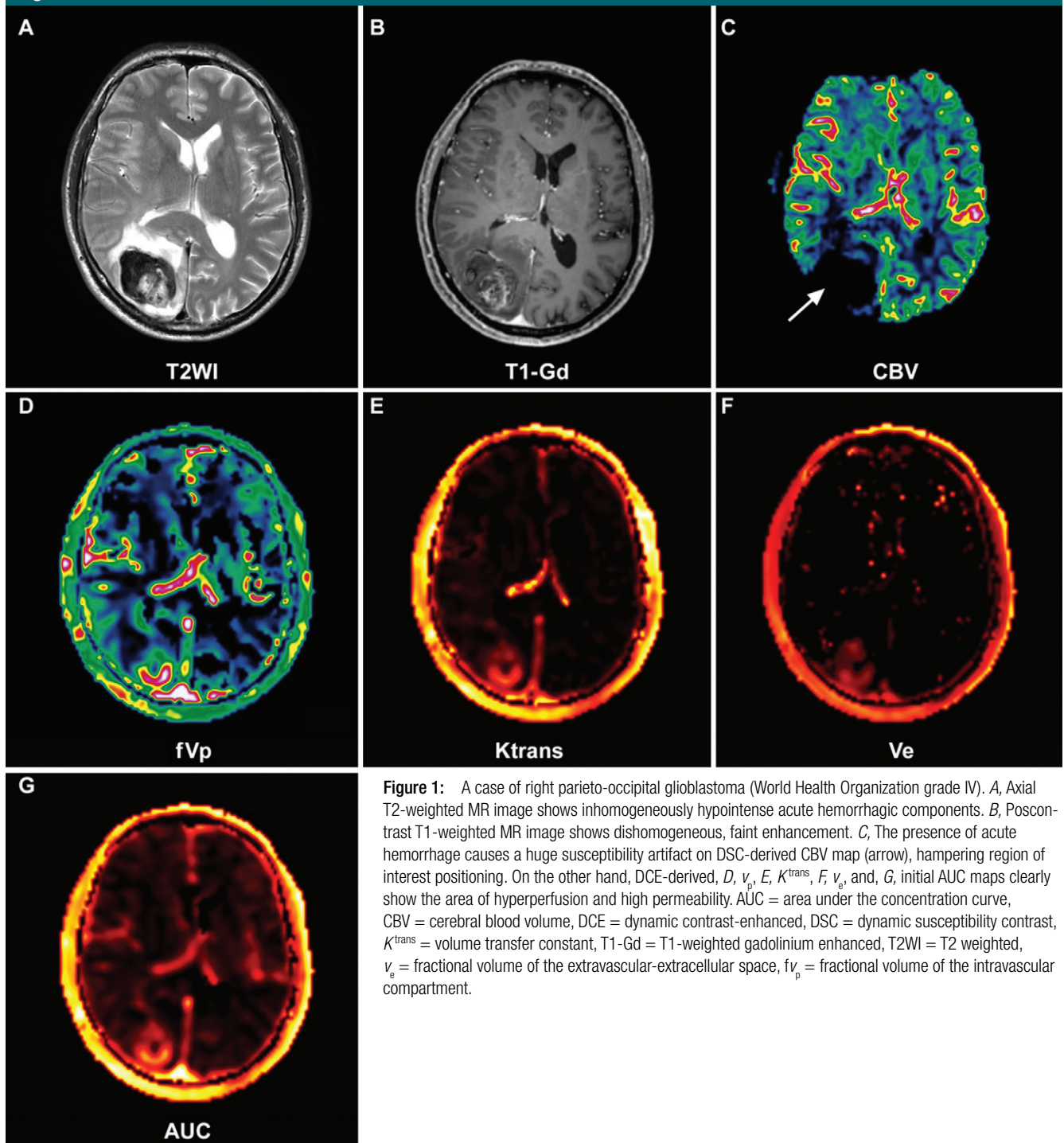


Figure 1: A case of right parieto-occipital glioblastoma (World Health Organization grade IV). *A*, Axial T2-weighted MR image shows inhomogeneously hypointense acute hemorrhagic components. *B*, Postcontrast T1-weighted MR image shows dishomogeneous, faint enhancement. *C*, The presence of acute hemorrhage causes a huge susceptibility artifact on DSC-derived CBV map (arrow), hampering region of interest positioning. On the other hand, DCE-derived *D*, v_p , *E*, K^{trans} , *F*, v_e , and *G*, initial AUC maps clearly show the area of hyperperfusion and high permeability. AUC = area under the concentration curve, CBV = cerebral blood volume, DCE = dynamic contrast-enhanced, DSC = dynamic susceptibility contrast, K^{trans} = volume transfer constant, T1-Gd = T1-weighted gadolinium enhanced, T2WI = T2 weighted, v_e = fractional volume of the extravascular-extracellular space, v_p = fractional volume of the intravascular compartment.

the analysis: Five patients because of inadequate DCE vascular input function deconvolution curves and one because of important susceptibility artifacts on DSC

images that hampered appropriate ROI positioning (Fig 1). Thus, 94 patients served as the final cohort for the analysis. Of these 94 patients, 79 underwent gross

tumor resection and 15 underwent stereotactic biopsy or subtotal resection.

Histopathologic analysis revealed that 28 of 94 patients had a low-grade

glioma (30%; WHO II), 23 patients had an anaplastic glioma (25%; WHO III), and 43 patients had a glioblastoma (45%; WHO IV). (Table E1 [online]).

Interreader Reproducibility

DSC- and DCE-derived measures had excellent interreader reproducibility, with intraclass correlation coefficients of 0.846 for v_p , 0.866 for K^{trans} , 0.782 for v_e , 0.873 for iAUC, and 0.858 for rCBV ($P < .0001$) (Table E2 [online]). Both readers agreed that ROI positioning was easier at qualitative assessment of DCE-derived maps than of CBV maps, especially in the evaluation of cortical tumors, mainly because of the easier discrimination of large vessels from true intralesional hotspots.

DCE- and DSC-derived Measures according to Glioma Grade

Median values of each hotspot parameter were significantly different between lower-grade gliomas (WHO II or III) and glioblastoma (WHO IV) ($P < .0001$) (Table 2 and Fig 2).

The median value of grade II and grade III gliomas was statistically different for DCE-derived v_p ($P = .0189$), K^{trans} ($P = .0037$), v_e ($P = .0037$), and iAUC ($P = .0037$) and for DSC-derived rCBV ($P = .0189$). Similarly, there was a statistically significant difference between grade III gliomas and

glioblastomas in terms of median values for v_p ($P = .0227$), v_e ($P = .0270$), iAUC ($P = .050$), and rCBV ($P = .0045$). The median K^{trans} values were not significantly different ($P = .0681$).

Each perfusion parameter had a highly significant positive correlation with respect to glioma grade, with ρ coefficients of 0.663 for v_p , 0.669 for K^{trans} , 0.708 for v_e , 0.683 for iAUC, and 0.737 for rCBV ($P < .0001$). The Spearman rank correlation test revealed significant relationships between intrapatient v_p and rCBV values ($\rho = 0.765$, $P < .0001$).

Accuracy of DCE- and DSC-derived Parameters for Distinguishing Glioma Grades

Table 3 shows A_z values, proportional to diagnostic accuracy, and the respective cutoff values of each DCE- and DSC-derived parameter for distinguishing lower-grade glioma (WHO II or III) from glioblastoma (WHO IV), according to the new WHO 2016 classification scheme. Among DCE-derived parameters, the v_p and v_e had the highest A_z (0.847 and 0.853, respectively). Cutoff values of 3.06 mL/100 g for v_p , 0.122 for iAUC, 0.045 min^{-1} for K^{trans} , and 16.23% for v_e were all associated with a sensitivity of 85.7% and an increasing specificity of 70.8%, 74.5%, 76.5%, and 78.4%, respectively (Table 3). For DSC, rCBV

had the highest A_z of 0.894, although this difference did not reach statistical significance ($P > .05$) compared with DCE parameters. An rCBV cutoff value of 6.71 allowed differentiation of lower-grade glioma from glioblastoma with 85.7% sensitivity and 80.4% specificity. The combination of all DCE-derived parameters and DSC-derived rCBV parameters outperformed the single DCE parameters alone ($P < .05$) but not rCBV ($P = .09$) (Fig 3a and Table E3 [online]).

For differentiating grade II from grade III or IV gliomas, according to the previous WHO grading system (Table 3), the DCE-derived K^{trans} , v_e , and iAUC had the highest A_z (0.903). Combining DCE- and DSC-derived parameters slightly improved the accuracy (Fig 3b and Table E3 [online]), but the differences were not statistically significant ($P > .05$).

Table E4 (online) shows the results of ROC analysis for differentiating WHO II from WHO III glioma and WHO III glioma from glioblastoma. For DCE-derived parameters, the A_z values for distinguishing grade II from grade III gliomas were generally higher, while for DSC-derived rCBV, the A_z for differentiating grade III gliomas from glioblastomas was the highest. However, none of the parameters fulfilled the selection criteria for cutoff value calculation as reported in the Statistical Analysis section.

Table 2

Hotspot Values of v_p , K^{trans} , v_e , iAUC, and rCBV for Different Tumor Grades

Parameter	WHO II (n = 28)	WHO III (n = 23)	WHO IV Glioblastoma (n = 43)	PValue*			
				II vs III†	II vs IV†	III vs IV†	II/III vs IV‡
v_p (mL/100 g)	0.805 (0.532–1.477)	3.247 (0.849–6.484)	6.707 (5.458–8.695)	.019 (.017)	<.0001 (<.0001)	.023 (.009)	<.0001 (<.0001)
K^{trans} (min^{-1})	0.004 (0.001–0.008)	0.040 (0.009–0.113)	0.079 (0.063–0.106)	.004 (.001)	<.0001 (<.0001)	.068 (.068)	<.0001 (<.0001)
v_e (%)	0.0 (0.0–0.0)	14.5 (0.0–28.4)	27.3 (20.22–35.58)	.004 (.002)	<.0001 (<.0001)	.027 (.016)	<.0001 (<.0001)
iAUC	0.02 (0.010–0.028)	0.13 (0.038–0.205)	0.20 (0.162–0.227)	.004 (.001)	<.0001 (<.0001)	.050 (.040)	<.0001 (<.0001)
rCBV	2.05 (1.534–2.516)	5.70 (2.411–8.825)	11.65 (8.873–13.42)	.019 (.019)	<.0001 (<.0001)	.004 (.001)	<.0001 (<.0001)

Note.—Unless otherwise indicated, data are interpatient median values, with range in parentheses. iAUC = initial area under the concentration curve, K^{trans} = volume transfer constant, rCBV = relative cerebral blood volume, v_e = fractional volume of the extravascular-extracellular space, v_p = fractional volume of the intravascular compartment, WHO = World Health Organization.

* $P < .05$ indicates a significant difference between groups. P values were adjusted for multiple testing by using the Benjamini-Hochberg correction; original, raw P values are in parentheses.

† Calculated by using Kruskal-Wallis and Dunn tests for multiple pairwise comparisons.

‡ Calculated by using Mann-Whitney U test.

Figure 2

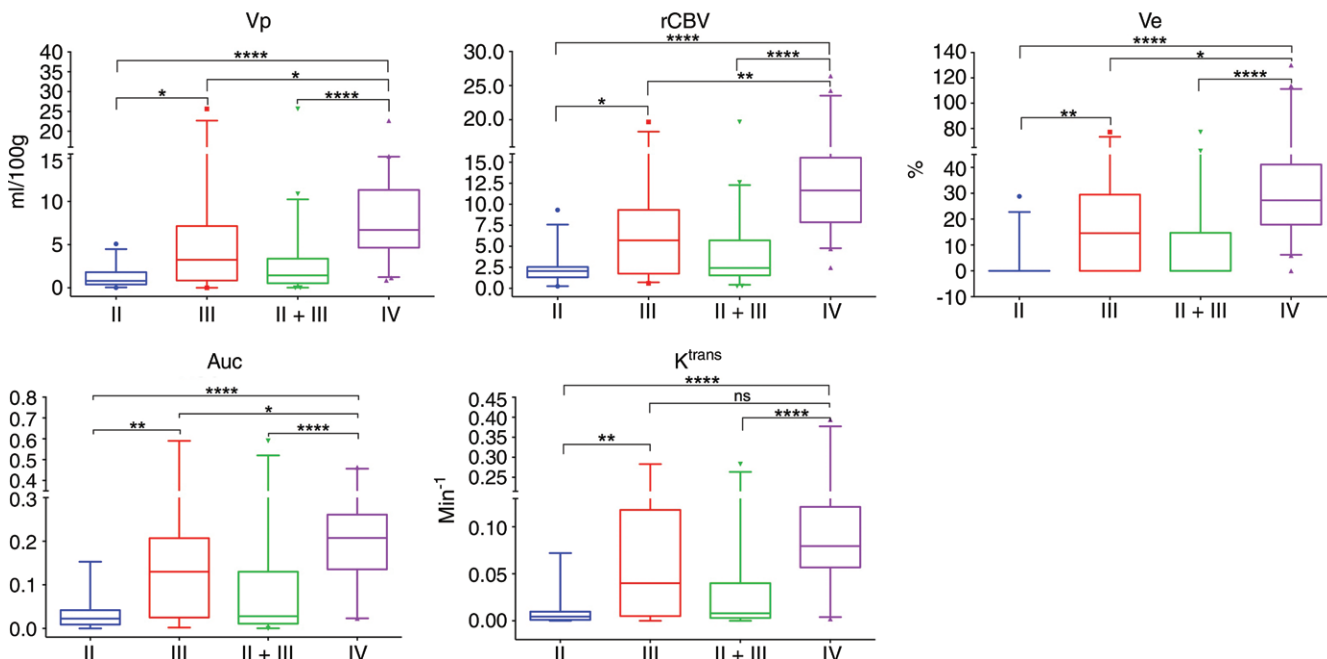


Figure 2: Highest abnormality (hotspot) values of DSC- and DCE-derived parameters for WHO grade II or III lower-grade glioma and WHO grade IV (glioblastoma). Boxplots show K^{trans} , v_e , $iAUC$, v_p , and $rCBV$ values in different tumor grades. Kruskal-Wallis and Dunn tests for multiple comparisons were used to assess group difference between median values of perfusion parameters in WHO II (blank), WHO III (dots), and WHO IV (squares) gliomas, and the Mann-Whitney U test was used to assess group differences in median values between lower-grade glioma (WHO II and III) (stripes) and glioblastoma (squares). * = $P \leq .05$, ** = $P \leq .01$, *** = $P \leq .001$, **** = $P \leq .0001$. DCE = dynamic contrast-enhanced, DSC = dynamic susceptibility contrast, K^{trans} = volume transfer constant, $rCBV$ = cerebral blood volume, v_e = fractional volume of the extravascular-extracellular space, v_p = fractional volume of the intravascular compartment, WHO = World Health Organization.

Table 3

ROC Results of v_p , K^{trans} , v_e , $iAUC$, and $rCBV$ Values and Their A_z and Cutoff Values for Glioma Grading

Comparison and Parameter	A_z value	Confidence Interval*	PValue	Cutoff Value	Sensitivity (%)	Specificity (%)
Lower-grade glioma (WHO II or III) vs glioblastoma (WHO IV)†						
v_p	0.847	0.769, 0.925	<.0001	3.06	85.7	70.8
K^{trans}	0.831	0.741, 0.921	<.0001	0.045	85.7	76.5
v_e	0.853	0.772, 0.934	<.0001	16.23	85.7	78.4
$iAUC$	0.842	0.760, 0.924	<.0001	0.122	85.7	74.5
$rCBV$	0.894	0.830, 0.958	<.0001	6.71	85.7	80.4
WHO II vs WHO III/IV glioma						
v_p	0.868	0.796, 0.939	<.0001	1.50	86.4	71.4
K^{trans}	0.903	0.841, 0.965	<.0001	0.015	86.4	85.7
v_e	0.903	0.838, 0.967	<.0001	1.75	87.9	85.7
$iAUC$	0.906	0.846, 0.965	<.0001	0.049	86.4	82.1
$rCBV$	0.898	0.833, 0.963	<.0001	3.33	86.4	85.7

Note.— $iAUC$ = initial area under the concentration curve, K^{trans} = volume transfer constant, $rCBV$ = relative cerebral blood volume, v_e = fractional volume of the extravascular-extracellular space, v_p = fractional volume of the intravascular compartment, WHO = World Health Organization.

* Data are 95% binomial exact confidence intervals.

† According to the WHO 2016 classification.

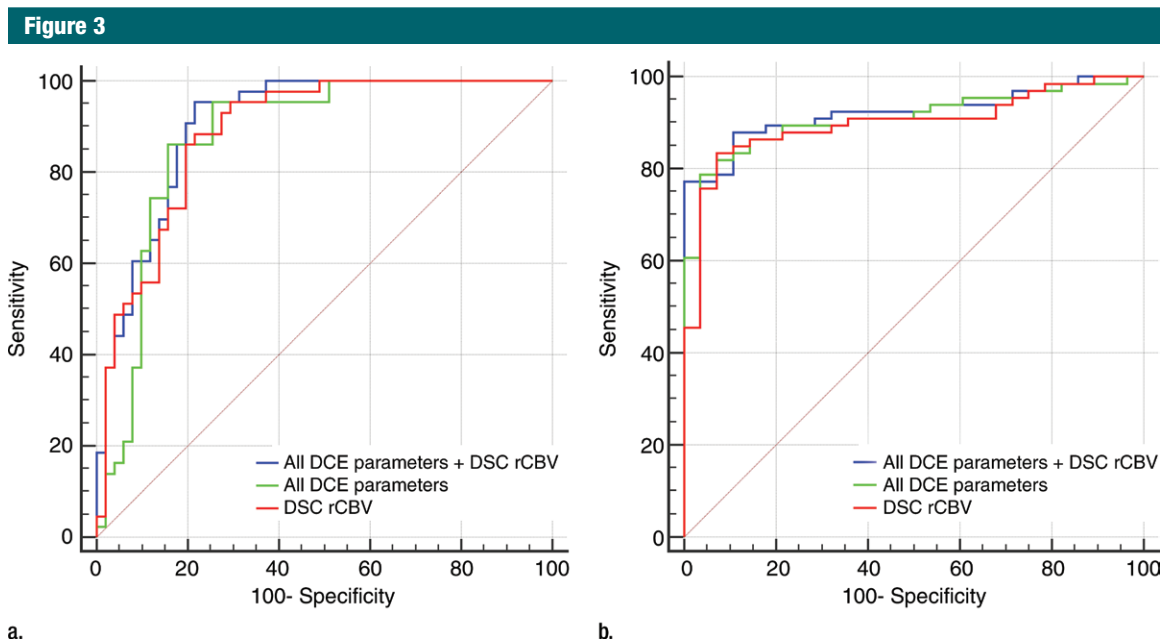


Figure 3: Graphs show comparison of ROC curves of (a) combined DCE and DSC hotspot values for differentiating (a) lower-grade glioma (WHO II/III) from glioblastoma (WHO IV) according to the new 2016 WHO classification scheme and (b) WHO II from WHO III or IV glioma according to the former WHO grading system. DCE = dynamic contrast-enhanced, DSC = dynamic susceptibility contrast, rCBV = cerebral blood volume, ROC = receiver operating characteristic, WHO = World Health Organization.

Table 4

Hotspot Values of v_p , K^{trans} , v_e , iAUC, and rCBV for Different Lower-Grade Glioma Molecular Subtypes

Parameter	IDH Mutation and 1p19q Codeletion (n = 13)	IDH Mutation but no 1p19q Codeletion (n = 14)	IDH Mutation (n = 27)	IDH Wild-Type (n = 9)	PValue*	
					IDH Mutation and 1p19q Codeletion vs Noncodeletion	IDH Mutation vs IDH Wild-Type
v_p (mL/100 g)	0.921 (0.222–2.944)	1.135 (0.369–5.247)	1.09 (0.532–1.829)	2.91 (0.363–7.461)	>.05	>.05
K^{trans} (min ⁻¹)	0.008 (0.003–0.280)	0.007 (0.001–0.118)	0.008 (0.003–0.012)	0.009 (0.004–0.091)	>.05	>.05
v_e (%)	0.0 (0.0–18.18)	0.0 (0.0–23.01)	0.0 (0.0–3.59)	0.0 (0.0–14.71)	>.05	>.05
iAUC	0.028 (0.009–0.073)	0.024 (0.002–0.173)	0.025 (0.011–0.063)	0.047 (0.017–0.168)	>.05	>.05
rCBV	1.99 (1.397–5.705)	1.83 (0.944–3.679)	1.98 (1.426–3.667)	2.53 (2.174–9.325)	.056	>.05

Note.—Data are interpatient median values, with ranges in parentheses. iAUC = initial area under the concentration curve, IDH = isocitrate dehydrogenase, K^{trans} = volume transfer constant, rCBV = relative cerebral blood volume, v_e = fractional volume of the extravascular-extracellular space, v_p = fractional volume of the intravascular compartment.

* $P < .05$ indicates a significant difference between groups. P values were calculated by using the Mann-Whitney U test.

DCE- and DSC-derived Markers according to Molecular Subtypes

Molecular markers used in the 2016 WHO classification were available for 67 of 94 patients. In these patients, 36% (13 of 36) of the lower-grade II and III gliomas were IDH mutant and 1p/19q codeleted, 39% (14 of 36) were IDH mutant without 1p/19q codeletion, and 25% (nine of 36) were IDH wild-type. Of the 31 glioblastomas with molecular

characterization, 30 were IDH wild-type (97%) (Table E1 [online]).

Among lower-grade gliomas (WHO II or III), the median values of each hotspot parameter did not reach a significant difference between IDH-mutated and IDH wild-type tumors, although both v_p and rCBV tended to be higher in the latter (Table 4). No significant differences in DCE- or DSC-derived perfusion parameters were found between IDH-mutant

tumors with and those without 1p19q codeletion ($P > .05$).

DSC- and DCE-derived Markers according to MR Imaging Equipment

Among the examinations in 94 patients included in the final analysis, 65 were performed with a Philips Achieva MR imaging unit, 19 with a Siemens Magnetom, and 10 with a GE Signa HDxt. No difference in DSC- and

DCE-derived median values was found between these groups according to tumor grade.

Discussion

In this study, we demonstrated the feasibility of a standardized protocol for acquisition and analysis of DSC and DCE MR imaging data in a multicenter clinical setting, with high reproducibility across different imaging MR equipment. The whole protocol was tolerated in all the recruited patients, and only a small number of patients were excluded from the analysis for technical reasons. Moreover, excellent interreader reproducibility of DSC- and DCE-derived measures was reported, further demonstrating the robustness of these techniques in the quantitative assessment of brain gliomas.

Large multicenter studies that correlate imaging findings with the new WHO 2016 brain tumor classification scheme (20) have still not been emphasized in the literature. According to this classification, a high diagnostic accuracy of DCE- and DSC-derived biomarkers in distinguishing lower-grade glioma (WHO II or III) from glioblastoma (WHO IV) was found in this multicenter series of patients (Table 3). Interestingly, although v_p , v_e , and rCBV had the highest A_z (0.847, 0.853, and 0.894, respectively), their behavior in terms of quantitative evaluation was similar with respect to WHO grade. Nonetheless, it is worth noting that both readers reported easier qualitative evaluation of DCE-derived v_p maps than CBV maps for ROI positioning, probably because of the presence of susceptibility artifacts often found on CBV maps in the proximity of large vessels, making the selection of reliable intralesional hotspots difficult, especially in cortical tumors. A significant correlation between the two intravascular compartment markers, v_p and rCBV, was also found in this study, thus confirming the potential role of this DCE-derived estimate of tumor neoangiogenesis in glioma grading (16,17).

A similar, high diagnostic accuracy of DCE- and DSC-derived parameters

in grading gliomas was found according to the former WHO classification scheme, which distinguishes low-grade (WHO II) from higher-grade (WHO III or IV) gliomas (Table 3), confirming the results of previous single-center studies, focused on selected parameters such as rCBV, K^{trans} , and v_p (16,17,23). Indeed, we found an rCBV cutoff value of 3.33 for grading gliomas according to this former classification, providing a sensitivity of 86.4% and a specificity of 85.7% (Table 3), which is in line with results of previous studies considering similar higher values of specificity (2). As expected, this cutoff is lower than the value of 6.71, referring to the differentiation between lower-grade gliomas and glioblastomas, according to the new 2016 WHO classification scheme.

Regarding the underlying biologic meaning of each parameter, our finding of a better accuracy of v_e in differentiating lower-grade gliomas from glioblastoma (Table 3) may reflect the higher mitotic activity of the latter, which is typical of more proliferative tumors (15). Moreover, v_e showed the highest accuracy in differentiating grade II from grade III gliomas (Table E2 [online]), and it was also associated with a better performance of K^{trans} over v_p and rCBV. These data could be related to lower neoangiogenesis in these tumors and to the presence of anomalous leaky vessels in enhancing grade III tumors, which represented the majority of our cases. In addition, the best performance in differentiating grade III gliomas from glioblastomas was shown by v_p and rCBV, probably related to an increase in microvascular density at least in part independent from vessel permeability as measured by K^{trans} (16).

The combination of all DCE-derived markers with rCBV did not significantly improve the diagnostic accuracy for grading gliomas, outperforming the single DCE parameters alone but not rCBV significantly (Fig 3 and Table E3 [online]).

A secondary aim of our study was to explore the correlation of DSC- and DCE-derived metrics with important

molecular alterations identified in the new 2016 WHO classification of gliomas (20). The requisite diagnostic biomarkers in this classification are IDH1/2 (IDH) mutations and 1p/19q codeletion. Particularly for lower-grade gliomas, it is well established that gene expression can significantly affect the disease course, with IDH-mutant tumors having a better prognosis than wild-type (24). Of note, in our study no significant differences in DCE- or DSC-derived parameters were found between IDH-mutant and IDH-wild-type lower-grade gliomas, although a moderate increase in both v_p and rCBV was evident in the latter. Furthermore, no significant differences were found between IDH-mutant tumors with and those without 1p19q codeletion. This may mean that a single imaging parameter is not able to capture the biologic complexity underlying molecular phenotypes in gliomas (25), which will need to be unraveled by multivariate radiogenomic analyses in the future (26,27).

Overall, our findings suggest that DCE and DSC techniques may be used independently by performing in an equivalent manner in the preoperative grading of gliomas. Thus, besides the aforementioned scarce sensitivity to susceptibility artifacts of DCE and its multifaceted quantitative evaluation of tumor vasculature, our data further promote the implementation of this technique in the clinical work-up of brain tumors as a possible valid and robust alternative to DSC. In addition, as the value of DCE has been recently highlighted in the follow-up of treated gliomas (4,28–31), it is of utmost importance to obtain robust baseline data as a reference (32).

This study had limitations. In particular, some issues still remain open regarding the quantification of perfusion parameters. We performed T1 mapping for voxelwise quantification of tumor tissue T1 values; although this is still debated, the strong acquisition and analysis reproducibility of our protocol fosters future implementation in its current form in the clinics.

Because this multicenter study was designed to show reproducibility

of acquisition and analysis and accuracy of DCE and DSC in grading gliomas according to the previous WHO classification, the initial sample size was calculated on the recruitment of 60 patients with WHO III or IV gliomas and 40 patients with WHO II gliomas. As a consequence, a possible limitation was the relative class imbalance in high-grade gliomas with a small number of WHO III cases that does not allow us to draw definitive conclusions on the differentiation of this subgroup from glioblastoma and low-grade gliomas.

Finally, because corticosteroids can affect BBB permeability, our results might not be fully generalizable to patients who have already been treated with steroids (33–35).

In summary, a standardized, multicenter acquisition and analysis protocol of DCE and DSC data is feasible and highly reproducible, with both showing a comparable high diagnostic accuracy in glioma grading according to the new WHO 2016 classification scheme.

Acknowledgments: The authors thank Antonella Iadanza, MSc, for technical support, and Giulio Pezzetti, MD, for help with data collection and processing.

Disclosures of Conflicts of Interest: N.A. Activities related to the present article: has received support for travel and fees for review activities from Bayer Healthcare. Activities not related to the present article: is a member of the advisory board of Bracco; is a consultant for Bayer Healthcare; is on the speakers bureaus of Bayer Healthcare and Guerbet. Other relationships: disclosed no relevant relationships. A. Castellano disclosed no relevant relationships. M. Cadioli Activities related to the present article: is an employee of Philips Healthcare. Activities not related to the present article: disclosed no relevant relationships. Other relationships: disclosed no relevant relationships. G.M.C. disclosed no relevant relationships. V.C. disclosed no relevant relationships. A.B. disclosed no relevant relationships. M.G. disclosed no relevant relationships. A. Costa disclosed no relevant relationships. G.G. disclosed no relevant relationships. P.V. disclosed no relevant relationships. D.A. disclosed no relevant relationships. M.R.T. disclosed no relevant relationships. V.T. disclosed no relevant relationships. B.J.E. disclosed no relevant relationships. M. Caulo disclosed no relevant relationships.

References

- Shiroishi MS, Castellazzi G, Boxerman JL, et al. Principles of T2*-weighted dynamic susceptibility contrast MRI technique in brain tumor imaging. *J Magn Reson Imaging* 2015;41(2):296–313 .
- Law M, Yang S, Wang H, et al. Glioma grading: sensitivity, specificity, and predictive values of perfusion MR imaging and proton MR spectroscopic imaging compared with conventional MR imaging. *AJNR Am J Neuroradiol* 2003;24(10):1989–1998 .
- Law M, Young RJ, Babb JS, et al. Gliomas: predicting time to progression or survival with cerebral blood volume measurements at dynamic susceptibility-weighted contrast-enhanced perfusion MR imaging. *Radiology* 2008;247(2):490–498 .
- Patel P, Baradaran H, Delgado D, et al. MR perfusion-weighted imaging in the evaluation of high-grade gliomas after treatment: a systematic review and meta-analysis. *Neuro Oncol* 2017;19(1):118–127 .
- Essig M, Nguyen TB, Shiroishi MS, et al. Perfusion MRI: the five most frequently asked clinical questions. *AJR Am J Roentgenol* 2013;201(3):W495–W510 .
- Welker K, Boxerman J, Kalnin A, et al. ASFN recommendations for clinical performance of MR dynamic susceptibility contrast perfusion imaging of the brain. *AJNR Am J Neuroradiol* 2015;36(6):E41–E51 .
- Hu LS, Kelm Z, Korfiatis P, et al. Impact of Software Modeling on the Accuracy of Perfusion MRI in Glioma. *AJNR Am J Neuroradiol* 2015;36(12):2242–2249 .
- Kelm ZS, Korfiatis PD, Lingineni RK, et al. Variability and accuracy of different software packages for dynamic susceptibility contrast magnetic resonance imaging for distinguishing glioblastoma progression from pseudoprogression. *J Med Imaging (Bellingham)* 2015;2(2):026001 .
- Conte GM, Castellano A, Altabella L, et al. Reproducibility of dynamic contrast-enhanced MRI and dynamic susceptibility contrast MRI in the study of brain gliomas: a comparison of data obtained using different commercial software. *Radiol Med (Torino)* 2017;122(4):294–302 .
- Heye AK, Culling RD, Valdés Hernández MC, Thrippleton MJ, Wardlaw JM. Assessment of blood-brain barrier disruption using dynamic contrast-enhanced MRI. A systematic review. *Neuroimage Clin* 2014;6:262–274 .
- Li X, Zhu Y, Kang H, et al. Glioma grading by microvascular permeability parameters derived from dynamic contrast-enhanced MRI and intratumoral susceptibility signal on susceptibility weighted imaging. *Cancer Imaging* 2015;15(1):4 .
- Patankar TF, Haroon HA, Mills SJ, et al. Is volume transfer coefficient (K(trans)) related to histologic grade in human gliomas? *AJNR Am J Neuroradiol* 2005;26(10):2455–2465 .
- Alcaide-Leon P, Pareto D, Martinez-Saez E, Auger C, Bharatha A, Rovira A. Pixel-by-Pixel Comparison of Volume Transfer Constant and Estimates of Cerebral Blood Volume from Dynamic Contrast-Enhanced and Dynamic Susceptibility Contrast-Enhanced MR Imaging in High-Grade Gliomas. *AJNR Am J Neuroradiol* 2015;36(5):871–876 .
- Nguyen TB, Cron GO, Bezzina K, et al. Correlation of Tumor Immunohistochemistry with Dynamic Contrast-Enhanced and DSC-MRI Parameters in Patients with Gliomas. *AJNR Am J Neuroradiol* 2016;37(12):2217–2223 .
- Mills SJ, du Plessis D, Pal P, et al. Mitotic activity in glioblastoma correlates with estimated extravascular extracellular space derived from dynamic contrast-enhanced MR Imaging. *AJNR Am J Neuroradiol* 2016;37(5):811–817 .
- Santarosa C, Castellano A, Conte GM, et al. Dynamic contrast-enhanced and dynamic susceptibility contrast perfusion MR imaging for glioma grading: Preliminary comparison of vessel compartment and permeability parameters using hotspot and histogram analysis. *Eur J Radiol* 2016;85(6):1147–1156 .
- Nguyen TB, Cron GO, Perdrizet K, et al. Comparison of the diagnostic accuracy of DSC- and dynamic contrast-enhanced MRI in the preoperative grading of astrocytomas. *AJNR Am J Neuroradiol* 2015;36(11):2017–2022 .
- Falk A, Fahlström M, Rostrop E, et al. Discrimination between glioma grades II and III in suspected low-grade gliomas using dynamic contrast-enhanced and dynamic susceptibility contrast perfusion MR imaging: a histogram analysis approach. *Neuroradiology* 2014;56(12):1031–1038 .
- Artzi M, Blumenthal DT, Bokstein F, et al. Classification of tumor area using combined DCE and DSC MRI in patients with glioblastoma. *J Neurooncol* 2015;121(2):349–357 .
- Louis DN, Perry A, Reifenberger G, et al. The 2016 World Health Organization Classification of Tumors of the Central Nervous System: a summary. *Acta Neuropathol (Berl)* 2016;131(6):803–820 .
- Tofts PS, Brix G, Buckley DL, et al. Estimating kinetic parameters from dynamic contrast-enhanced T(1)-weighted MRI of a diffusable tracer: standardized quan-

- titles and symbols. *J Magn Reson Imaging* 1999;10(3):223–232 .
22. Boxerman JL, Schmainda KM, Weisskoff RM. Relative cerebral blood volume maps corrected for contrast agent extravasation significantly correlate with glioma tumor grade, whereas uncorrected maps do not. *AJNR Am J Neuroradiol* 2006;27(4):859–867 .
 23. Larsson C, Kleppestø M, Rasmussen I Jr, et al. Sampling requirements in DCE-MRI based analysis of high grade gliomas: simulations and clinical results. *J Magn Reson Imaging* 2013;37(4):818–829 .
 24. Cancer Genome Atlas Research Network, Brat DJ, Verhaak RG, et al. Comprehensive, integrative genomic analysis of diffuse lower-grade gliomas. *N Engl J Med* 2015;372(26):2481–2498 .
 25. Castellano A, Falini A. Progress in neuroimaging of brain tumors. *Curr Opin Oncol* 2016;28(6):484–493 .
 26. Kickingereder P, Bonekamp D, Nowosielski M, et al. Radiogenomics of glioblastoma: machine learning-based classification of molecular characteristics by using multiparametric and multiregional MR imaging features. *Radiology* 2016;281(3):907–918 .
 27. Wiestler B, Kluge A, Lukas M, et al. Multiparametric MRI-based differentiation of WHO grade II/III glioma and WHO grade IV glioblastoma. *Sci Rep* 2016;6(1):35142 .
 28. Artzi M, Liberman G, Nadav G, et al. Differentiation between treatment-related changes and progressive disease in patients with high grade brain tumors using support vector machine classification based on DCE MRI. *J Neurooncol* 2016;127(3):515–524 .
 29. Kickingereder P, Wiestler B, Graf M, et al. Evaluation of dynamic contrast-enhanced MRI derived microvascular permeability in recurrent glioblastoma treated with bevacizumab. *J Neurooncol* 2015;121(2):373–380 .
 30. Larsen VA, Simonsen HJ, Law I, Larsson HB, Hansen AE. Evaluation of dynamic contrast-enhanced T1-weighted perfusion MRI in the differentiation of tumor recurrence from radiation necrosis. *Neuroradiology* 2013;55(3):361–369 .
 31. Thomas AA, Arevalo-Perez J, Kaley T, et al. Dynamic contrast enhanced T1 MRI perfusion differentiates pseudoprogression from recurrent glioblastoma. *J Neurooncol* 2015;125(1):183–190 .
 32. Nguyen TB, Cron GO, Mercier JF, et al. Preoperative prognostic value of dynamic contrast-enhanced MRI-derived contrast transfer coefficient and plasma volume in patients with cerebral gliomas. *AJNR Am J Neuroradiol* 2015;36(1):63–69 .
 33. Ostergaard L, Hochberg FH, Rabinov JD, et al. Early changes measured by magnetic resonance imaging in cerebral blood flow, blood volume, and blood-brain barrier permeability following dexamethasone treatment in patients with brain tumors. *J Neurosurg* 1999;90(2):300–305 .
 34. Neuwelt EA, Barnett PA, Bigner DD, Frenkel EP. Effects of adrenal cortical steroids and osmotic blood-brain barrier opening on methotrexate delivery to gliomas in the rodent: the factor of the blood-brain barrier. *Proc Natl Acad Sci U S A* 1982;79(14):4420–4423 .
 35. Bastin ME, Carpenter TK, Armitage PA, Sinha S, Wardlaw JM, Whittle IR. Effects of dexamethasone on cerebral perfusion and water diffusion in patients with high-grade glioma. *AJNR Am J Neuroradiol* 2006;27(2):402–408 .